Peter A. Bandettini, Ph.D.

Integration of fMRI Interpretation, Methodology, Technology, and Applications

Unit on Functional Imaging Methods

Laboratory of Brain and Cognition, NIMH

Introduction – from neuronal activity to fMRI contrast

Over ten years ago, the first papers appeared on functional magnetic resonance imaging (fMRI). The rapid growth of fMRI as a tool for non-invasively visualizing dynamic, localized neuronal processes in the human brain that followed reflects its promise for opening up new avenues of research in cognitive neuroscience and subsequent clinical applications. The evolution of fMRI can be viewed as a progression along four interacting themes: Interpretation, Methodology, Technology, and Applications. Since the Unit on Functional Imaging Methods, (UFIM), was established in March of 1999, its research focus has been balanced across these themes. This integrative philosophy is rooted in a belief that novel fMRI applications can best be carried out by researchers who are grounded with an understanding of the interpretation of the signal and the latest methodology and technology. In turn, advancements with the greatest impact in fMRI interpretation, methodology, and technology can be made most effectively by researchers that possess a firm understanding of the most relevant applications desired. UFIM has as a goal to recruit and train individuals where the collective expertise is a balance among these themes. The diverse expertise of UFIM members includes but is not limited to biomedical engineering, MRI physics, and cognitive neuroscience. The integrative research carried out by UFIM is only possible by a close collaborative interaction among these diverse backgrounds. Figure 1 illustrates the four themes, an approximate range of expertise among the types of fMRI researchers, and the approximate research focus of each of the individuals contributing to projects in this summary.

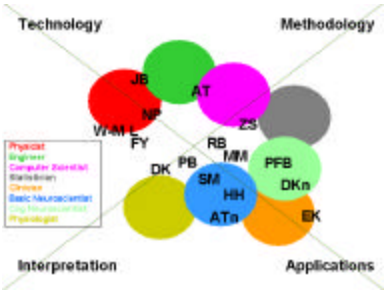

Figure 1: Schematic depiction the themes of fMRI advancement, the general interest of each type of fMRI researcher, and the research focus of the individuals (as indicated by the initials of their names) in UFIM and immediate research collaborators within FMRIF. My intent is the development and maintenance of a group that advances fMRI through active interaction among each research focus.

The ultimate goal of UFIM is the implementation of fMRI towards increased understanding the functional organization and physiology of the healthy and diseased human brain. Toward accomplishing this goal, the primary focus of UFIM is to more fully characterize the relationship between neuronal activity and fMRI signal changes. Full characterization of the relationship between neuronal activity and fMRI signal changes requires knowledge of all the factors that influence the fMRI signal as well and its variability across all relevant spatial and temporal scales of measurement. For fMRI to advance, the ability for precise inferences about brain activity across voxels, regions in the brain, individuals, and populations is necessary. More precise inferences about temporal dynamics across several time scales is also necessary.

The overall objectives of the summarized research are: 1) To develop a voxel-wise quantitative model of the relationship between neuronal activity and the fMRI signal change by modulating each relevant component (i.e. stimulus characteristics, pulse sequence weighting, physiologic state). 2) To develop techniques for the optimal estimation of individual components (i.e. hemodynamic response magnitude, latency, width, resolution, and random fluctuations). 3) To apply the most sensitive techniques available (including multi-channel phased array surface coils) for direct measurement of neural currents using MRI, and to test these techniques both in-vivo and in humans. 4) To exploit these developed techniques and insights to better understand neural processes with fMRI (i.e. lexical processing, and correlates to skin conductance changes).

The goals of UFIM are synergistic with those of the functional MRI facility (FMRIF), for which I am also the director. The primary purpose of a core facility is to advance the scientific research of the users – yet, at the same time, strive to create more robust methods and powerful imaging technology. To help to meet this goal, a fraction of each core facility individual's efforts is devoted to basic research, often in collaboration with members of UFIM. FMRIF strives to implement our understanding of the underlying basis of the fMRI signal towards the creation of more robust methods and powerful imaging technology and to make those methods available to the entire NIH. At the introduction to each theme, an overview of the specific projects, their goals, and their hypotheses will be given. In addition, the cross-project interactions will be included where applicable.

Theme 1: Interpretation

1A. Introduction: Unknowns regarding fMRI contrast.

Several types of physiologic information can be mapped using fMRI. This information includes baseline cerebral blood volume[1, 2], changes in blood volume [3], baseline and changes in cerebral perfusion [4-7], and changes in blood oxygenation [8-11]. Recent advances in calibration techniques have allowed measures of $CMRO_2$ changes [12-14]. Preliminary results suggest that the potential exists for quantitatively mapping blood volume [15] and blood oxygenation [16] non-invasively.

The physical basis of blood oxygenation level dependent (BOLD) contrast is oxygenation-dependent magnetic susceptibility of hemoglobin. Deoxyhemoglobin is paramagnetic, causing slightly attenuated baseline signal intensity in MRI image voxels containing deoxygenated blood. During brain activation, localized increases in blood flow outweigh the metabolically driven extraction of oxygen from the blood, causing an increase in blood oxygenation and consequently, a reduction in deoxyhemoglobin. This causes the MRI signal to start to increase about 2 s after activity begins. The signal plateaus in the "on" state after about 7 to 10 s, remaining elevated while the activity continues. When activity ends, the signal returns to baseline after about 8 to 11 s. Transient signal changes are also described, including a 'pre-undershoot' (reduced BOLD signal within the first two s of activity) and a more commonly observed 'post-undershoot' (reduced signal for 10 to 40 s after activity ends). It is accepted that localized increases in BOLD contrast reflect increases in neuronal activity but it has not been established to what degree of precision we can characterize neuronal activity from these signal changes.

Two primary unknowns remain about the interpretation of fMRI signals: 1) the quantitative relationship between neural activity and BOLD contrast, and 2) the biological mechanism underlying this relationship. The aim of Theme 1 is to address the first unknown, (see Figure 2). Progress in Theme 1 has been made by careful modulation of each component in Figure 2 (neuronal activation, hemodynamics, pulse sequence weighting) as well as direct, simultaneous and/or spatially registered measurements of neuronal activity and sources of noise. Models to describe these relationships have provided insight; however they are underdetermined in that most of the model parameters vary on a voxel-wise basis and therefore depend on the location and scale of measurement. A methodological goal, discussed in Theme 2, is to determine ways to characterize these variables on a voxel-wise basis and use this characterization to "calibrate" the fMRI signal changes. The concept behind the issues of heterogeneity are depicted in the lower half of Figure 2 which shows that the relevant neurophysiology of the brain is highly heterogeneous over space as well as across the spatial scale at which it is measured. In addition, the sources and degree of temporal variability, also not fully characterized, may vary across time scales.

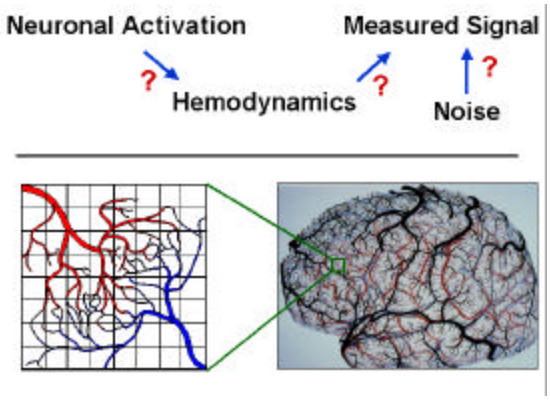

Figure 2: Depiction of the relationship between neuronal activity and measured signal changes. These relationships vary over spatial scale as each voxel contains different vasculature and tissue content. A primary goal of UFIM is to clarify these relationships and their variability over space, spatial scale, subject, subject population, and time. A secondary goal, inclusive in the methods theme, is to then devise methods to either "calibrate" the signal or extract further neuronal and physiologic information from fMRI time series. Third, the intent is to use the latest technological and methodological advancements towards addressing neuroscience and clinical questions more effectively – in applications.

The general approach taken by UFIM to address the issues of Theme 1 has been to modulate either neuronal activity or the pulse sequence (and therefore the relative vasculature being observed) and to map the effect on the signal magnitude and dynamics – thereby drawing inferences about how neuronal activity is reflected in the signal. A focus by UFIM is to characterize the spatial heterogeneity of the signal changes and determine the spatial correlation with each other (i.e. latency vs. linearity) and with other measures reflecting spatially

heterogeneous hemodynamics and/or neuronal activity (i.e. perfusion vs. BOLD changes) such that hemodynamic effects might be separated from neuronal effects. In addition, UFIM has begun to make use of independent measures sensitive to relevant neuronal events such as single-unit recordings, magnetoencephalography, and electroencephalography; as well as physiologic measures including as heart rate, respiration rate, skin conductance, pupil dilation, blood pressure, and hematocrit either simultaneously or in a similar experimental setting to further establish these relationships.

The underlying hypothesis of our work is that by modeling and empirical verification of the sources of variability in the BOLD response to calibrated stimulus conditions across a range of spatial and temporal scales, the physiological models relating blood oxygenation and perfusion to the neural signal will be more tightly constrained. Our initial focus was on spatial extent and the spatial distribution of non-linearities

1B. Progress Report

1B-1. The spatial extent of BOLD contrast.

Many studies on BOLD signal properties have focused on the temporal dynamics or on the spatial localization of the BOLD responses relative to the location of neuronal activation. However, few studies have addressed the question of what the true spatial extent or volume of the BOLD response to neuronal stimulation is despite the extensive use of such a metric in many imaging studies.

In an fMRI scanning session, the signal to noise ratio (SNR) is the limiting factor in determining the full extent of brain activation. Activated voxels with low SNR may not be statistically distinguishable from inactivated counterparts. In most fMRI experiments, thresholds for detecting activated voxels are set to minimize false positive (type I) errors, whereby an inactive voxel is incorrectly classified as activated. The result of such high specificity for activated voxels is a loss of sensitivity, in which an undetermined number of activated voxels go undetected (false negatives, type II error). Such type II errors result in an underestimation of the spatial extent of the BOLD response. To determine the full spatial extent of the BOLD response, one needs to detect low SNR voxels (reduce type II error) without increasing the rate of false detection (keep type I error constant). This is achieved simply by collecting more data samples without further constraining the statistical model with presumptive information on the BOLD response or noise.

The goal of this study extends beyond methodology (determining the true spatial extent of BOLD) in that areas showing much more subtle and extensive activation within activated visual areas lends insight into the type of neuronal activity that BOLD contrast is sensitive to. A wider measured extent of activation may occur in response to local field potential (LFP) changes caused by the subthreshold activity of long-range horizontal connections [17, 18]. Using optical imaging techniques and extracellular electrodes, it has been shown that neural spiking accounted for 5% of the activated area detected with optical dyes, with the remaining 95% due to subthreshold activity [17]. Logothetis et al. have also presented direct evidence suggesting that BOLD signals correlate more with LFP than with neuronal spiking alone [19].

Recently, Huettel and McCarthy [20] examined the spatial extent of the BOLD response as a function of the number of averaged single trial stimulations and found the volume of activation to increase exponentially with averaging. However, it was unclear whether such increases would occur with block design stimulation that induce much higher SNR responses when compared with single trial stimulation.

In this study [21], we examined, using a block design, the spatial extent of the BOLD response to visual stimulation in normal volunteers by collecting multiple repetitions of the same scan and examining the extent of the BOLD response across repetitions and with increased averaging. We used gradient-echo EPI to image the BOLD response in the visual cortex. The imaged volume consisted of 18-24 axial slices 4 mm thick and an in plane resolution of 3.75x3.75 mm and TR=2000 ms. We define a scan as the time series of 100 volumes obtained simultaneously during one 200 s stimulus presentation period. Data were obtained at 1.5 T and 3 T. In a 200 s scan, the stimulus was presented for 20 s (ON) followed by 20 s of fixation only (OFF).

We found that with increased number of averages, a continual increase in the spatial extent of activation was observed. Figure 3a shows the volume of activation *(Va)* versus the averaging level *Navg* for data obtained at 3T

using a small stimulus (2.2 to 3.6 degrees eccentricity). Positive and negative BOLD volumes are marked by the '+' and black dot symbols respectively. For the positive BOLD response, increases of 50% of the initial volume occurred by averaging two scans, and increases of 100% occurred by averaging 4 or 5 scans. Increased averaging beyond that resulted in steady but smaller increases in activation volume. This study contrasts with that of Huettel and McCarthy in that the increase in the spatial extent is significantly larger than what their study implied.

With increased averaging, it is understood that voxels containing signal will exhibit an increase in the cross correlation coefficient, while those with no signal exhibit little change in either direction. Thus, the distribution of voxels containing signal will migrate to the right and further separate from the distribution of noise-only voxels. Figure 3b shows the rootogram envelope of the cross-correlation coefficients for different averaging levels *Nav*g. The rootogram, which is the square root of the histogram, is used to enhance the changes in the tail of the distribution. The black bar indicates the threshold used to classify voxels as activated. The different colors code for the averaging level from which the distribution was obtained. With increasing *Nav*g, the frequency of voxels with higher correlation coefficient increased as expected and the frequency of voxels with very low correlation coefficient decreased, indicating the presence of numerous voxels that contain signal with very low SNR. Intriguingly, we found that even after 22 scans, a large number of voxels were still migrating towards significance, as shown in the voxels to the right of a correlation coefficient of about 0.2 in Figure 2b. This suggests not only that a significantly larger region of the brain is activated than with the typical 5 scans that are performed on most studies, but also that perhaps the true volume of activation may be estimated by adding to the voxels above significance those that are moving towards significance.

Maps of these weak activations show that, while they do not extend beyond the visual cortex, they do extend to fill it's entire visual field representations, beyond the volume typically found to be activated by the annulus used. These data support the hypothesis that BOLD is sensitive to more extensive subthreshold activity. The large extent of BOLD activation may simply be caused by a large spread of the hemodynamic response to localized activation with the largest increases closest to the site of activation and decreasing responses farther away or by dephasing effects from weak gradients in a distal network of large venous vessels as opposed to proximal capillary effects. Based on the assumption that downstream vein effects typically show longer hemodynamic delays [22], we compared these results with latency measures on a voxel-wise basis. We found that the areas that showed the smallest degree of signal change or, rather, those areas that only passed significance after many averages, did not demonstrate a significant shift in hemodynamic latency, indicating that they are not likely to be downstream draining vein effects. We are ruling out this possibility by performing the same experiment using spin-echo sequences, which are insensitive to these spatially extensive gradients.

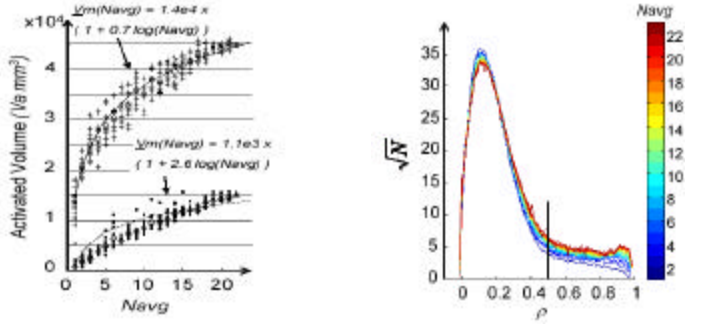

a. **b.**

Figure 3: a. Volume of activation *(Va)* versus averaging level *Navg* for the small stimulus. Positive and negative BOLD volumes are marked by the plus symbols and black dot symbols, respectively. b. Rootogram envelopes of the cross-correlation coefficients, r, for different averaging levels *Nav*g. The black vertical bar indicates the threshold used to classify voxels as activated ($p < 0.0001$). Different colors code for the averaging level at which the distribution was obtained.

1B-2. The spatial heterogeneity of the BOLD response non-linearity.

The utility of fMRI is directly related to the degree to which neuronal activation can be implied through these hemodynamic changes and resulting effects on MRI contrast, most importantly, blood oxygenation level dependent (BOLD) contrast. An important step in characterizing the relationship between the neuronal firing and measured fMRI signal is by assessment of the linearity of the measured BOLD signal in response to neural stimulation. While recent studies have suggested that, at *steady state* (i.e. activation lasting for longer than 10 s) the BOLD response shows a proportionality to neuronal firing rate [23] or implied measures of task intensity

[10, 24-26], the *dynamic* BOLD response, meaning the magnitude of response as a function of task durations less than 5 s, has been shown to have highly nonlinear behavior. The BOLD response does not obey superposition for certain stimuli [27-29]. While longer duration stimuli behave in an approximately linear fashion, short duration stimuli produce responses larger than predicted from a linear model.

Linearity is presumed in many analysis procedures and the determination of any deviation from this linearity is crucial in a more precise quantitation of neuronal activity. The source of the observed nonlinear behavior of the BOLD signal has not yet been clearly determined. We attempt to clarify the source of these dynamic nonlinearities by comparison of our results with hemodynamic measures as well as results using single-unit recordings reported in the literature.

The observed fMRI response to a stimulus is the resultant of two cascaded responses. The stimulus first triggers a neural response which, in turn triggers a hemodynamic response that is monitored by fMRI. Thus, the non-linearity of the BOLD signal could arise from either a nonlinearity in the neuronal response, a nonlinearity in the hemodynamics, or both. Studies have shown that in certain cases the neuronal response is not linearly related to the stimulus duration. Visual stimuli presented with a step function time course, for example, cause neurons to fire rapidly with the onset of the stimulus followed by a lower firing rate [30-32]. Other recent studies suggest that the nonlinearity may also arise from the complex hemodynamics, (i.e. differences in timing of blood volume, oxygenation, and metabolism changes) involved in producing the BOLD signal [33].

The objective of this study was to characterize the spatial heterogeneity of the nonlinear behavior of the BOLD signal. The hypothesis was that if the hemodynamics are the dominant source of this nonlinear behavior, then a measure of the degree of nonlinearity would likely to be correlated with measures that are influenced by the vasculature, such as the onset latency or response magnitude. In this section we describe experiments in which a dynamic analysis of the spatial heterogeneity of response is adopted rather than steady-state analysis used for the study of spatial extent described in the previous section.

The linearity of the fMRI BOLD response with respect to stimulus duration (the "ON" period) was assessed in two tasks – a motor task consisting of bilateral finger tapping, and a visual task in which the subject passively viewed an 8 Hz contrast reversing checkerboard. The visual stimuli were presented at durations of 250 ms, 500 ms, 1000 ms, and 2000 ms; and the finger tapping was performed at durations of 500 ms, 1000 ms, 2000 ms, and 4000 ms. Images were also acquired in a blocked trial paradigm, alternating eight 20 s periods of stimulation with eight 20 s periods of rest for a total duration of 320 s. During these tasks, a series of 320 echo-planar images (EPI) were acquired on a 3T GE (Waukesha, WI, USA) magnet, equipped with a local birdcage RF coil (Medical Advances, Milwaukee, WI, USA). Eight axial slices with a 24 cm field of view and 5 mm slice thickness were used to cover the visual cortex during the visual task and the motor cortex during the finger tapping task. In each voxel, the area of the averaged response to these tasks or stimuli was divided by the stimulus duration to produce a measure of linearity – the output of the system for a given level of input. This value was normalized by the area of the fMRI response to a blocked design in order to show how much larger the measured response is compared to that of a linear system. The measure of nonlinearity in voxels with significant activation was then compared with the activation amplitude and latency, both strongly influenced by hemodynamic variability on a voxel-wise basis.

In agreement with previous studies, the BOLD response was found to be nonlinear, with activation amplitudes larger than predicted from a linear model at shorter stimulus durations. This nonlinearity was found, as shown in Figure 4, to vary considerably over space, with some regions showing a response 8 times larger than predicted from a linear system for a 250 ms visual stimulus, while other areas only showed a 2 times larger response. For the finger-tapping task, a distinct difference between the degree of nonlinearity in the primary and supplementary motor areas was observed. This measure, however, was not significantly correlated with either the response magnitude or latency, for both visual and motor tasks.

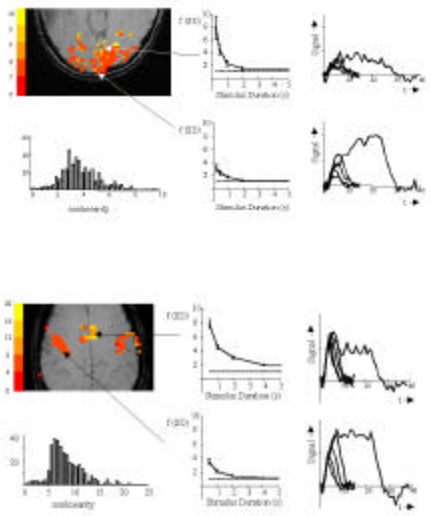

a

b

Figure 4: Nonlinearity of the BOLD response in one slice of the a. visual cortex in response to a contrast reversing checkerboard presented for different durations, and b. motor cortex in response to various durations of bilateral finger tapping. The amount by which the response is greater than a linear model at each stimulus duration is shown as a curve for two voxels. Responses are larger at shorter stimulus durations than predicted from a linear system. Averaged responses to the brief stimuli for the corresponding voxels are shown on the right. A histogram of computed nonlinearities is shown on the bottom. A considerable variation in the nonlinearity is observed across voxels and, most clearly between primary and supplementary motor cortex. This variation in nonlinearity is highly reproducible and does not correlate with hemodynamic latency or magnitude.

The lack of correlation between the measure of nonlinearity and indicators of vascular architecture suggests that the observed nonlinearity is not of vascular origin. Instead, the degree of nonlinearity appears to correspond more to variations in functional specialization, for example, in the primary and supplementary motor cortex. These results suggest that perhaps initiation of action corresponds to a larger initial transient or a longer minimum processing time in supplementary motor cortex than in primary motor cortex. The existing implication of this work is that the maps in Figure 4 may directly reflect the initial transient neuronal activity magnitude. Future work will involve verification of these findings using more better defined and understood stimuli.

1C. Current and Future Experiments

1C-1. Inverse modeling of BOLD to extract transient neuronal activity.

The nonlinear dependence of the BOLD signal amplitude on the stimulus duration can result from a nonlinear neuronal response to a particular stimulus. Studies employing direct electrical recordings in monkey and cat cortex have shown that a population of neurons will often fire more rapidly immediately after the onset of a stimulus, decreasing to a reduced level of activity for longer stimulations. Albrecht *et al.* reported that the neuronal response of the cat striate cortex during sustained high contrast stimuli decayed from a peak response to a sustained plateau response [30]. The exponential fit of the decay had a time constant between 0.5 and 2.0 s. Bonds *et al.* found that neuronal response gain adjustment occurs with longer time constants, typically 5-7 s but as brief as 3 s [31]. Maddess *et al.* estimated a ratio of 3:1 for the change in the firing rate between the stimulus onset and 6 s post-stimulus onset [32]. This initial transient is also observed in simultaneous electrical and BOLD recordings in monkeys [19] which clearly shows higher single- and multi-unit activity and LFPs in the first few seconds after the onset of a visual stimulus.

The degree to which this purely neuronal mechanism can account for the observed nonlinearity in the BOLD response can be evaluated by estimating the neuronal input required to produce the measured BOLD responses for the different duration stimuli, under the assumption that the hemodynamics are linear. This was done by subtracting the response to the shorter duration stimuli from the response to the longer duration stimuli, and comparing the amplitude of the residual to the shorter duration response.

As shown in Figure 5, the estimated neuronal activity showed a large initial period of activation followed by a decrease to a steady state level over a period of 1-2 s. The amplitude of the initial transient and the time constant of the decay are highly similar to direct measurements of LFPs in monkeys viewing a rotating checkerboard. We investigated further the hypothesis that the nonlinearity in the BOLD response is dominated by neuronal transients by measuring the BOLD response to the presentation of static gratings, which have been shown to produce much shorter transients lasting only a few 100 ms in direct recordings of electrical activity in

monkeys. The amplitudes of the BOLD responses to brief stimuli in our study were consistent with a large transient overshoot in the neuronal activity in the first few 100 ms following the presentation of the stimulus, again in agreement with direct electrical recordings. Of course, these results are preliminary in that a simple resemblance does not prove that we are observing the same phenomenon. Currently, we are researching stimuli to use such that these initial transient effects may be more robustly and accurately modulated and compared across regions. Our hypothesis that changes or spatial differences in the hemodynamically derived transients are due to neuronal transient signal and not hemodynamics will be tested by observing if the derived transients change with the modulation in the input or vary spatially in a manner that corresponds to known functional segregation of these transients.

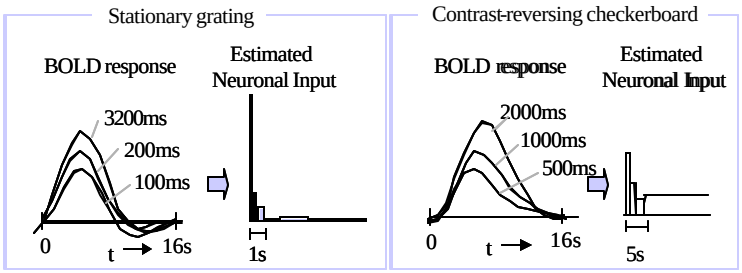

Figure 5: The fMRI BOLD response is nonlinear, with amplitudes larger than expected from a linear response to a boxcar input at shorter stimulus durations. The estimated neuronal input derived from the measured BOLD responses for different stimulus durations that can explain the larger than expected responses for brief stimuli.

1C-2. Dependence of BOLD response amplitude on stimulus duty cycle.

The dynamics of the BOLD fMRI signal is determined by not only the adaptation during the stimulus (the "ON" period), but also the recovery after stimulus cessation (the "OFF" period). This recovery is governed by the refractory period of the neurons [34] and possibly hemodynamic factors, such as a prolonged elevation of blood volume relative to the blood flow [35]. A study of these additional dynamics can therefore provide more information about underlying vascular and neuronal mechanisms.

As shown in Figure 6, measurements of the BOLD response to different stimulus OFF periods (alternating checkerboard relative to a black screen and fixation point) revealed that the signal behaved approximately linearly for stimulus OFF periods greater than 4 s, but nonlinearly at shorter OFF periods, with signal decreases *less* than expected from a linear model. This finding is inconsistent with dynamics resulting from a delayed blood volume response, suggesting that the principal mechanism is either a nonlinear blood flow response to the neuronal activation, a nonlinear neuronal response to the stimulus, or both. A transient increased signal observed in some areas following cessation of the stimulus further supports a neuronal mechanism

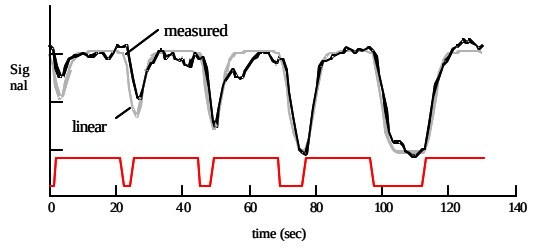

Figure 6: Measured BOLD response (dark line) and ideal linear prediction (gray line) for visual stimulation with "OFF" periods of 2, 3, 4, 8, and 16 s. For short "OFF" durations, the BOLD decrease is smaller than predicted.

The results of this study, combined with the observation that brief stimulations produce larger signal increases than a linear prediction, also suggest that the amplitudes of the measured BOLD signal changes depend on the ratio of brief stimulation periods to brief control periods – in other words, the fraction of time spent stimulating versus that in the control condition. This hypothesis was tested by presenting a contrast reversing checkerboard in an event-related paradigm with a varying ISI at three different fractions of stimulation time: 25%, 50%, and 75%. The amplitude of the deconvolved responses indeed showed a correlation with the stimulus duty cycle, with a larger response for infrequent stimulation, compared to more frequent stimulation, as shown in Figure 7. Furthermore, linear extrapolation of the deconvolved response to 75% stimulation underestimated the response to a blocked stimulus, whereas extrapolation of the deconvolved response from a run with 50% in the ON state fairly accurately predicted the response to the longer duration stimulus.

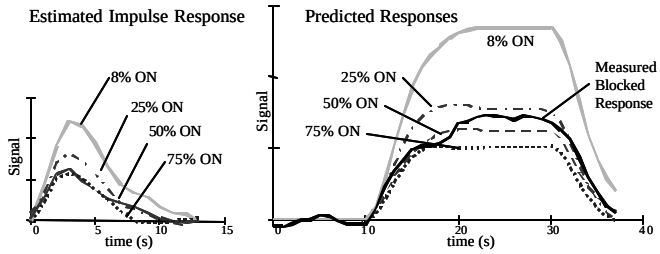

Figure 7: Estimated impulse response (left) and predicted responses to a 20-s duration stimulus (right) compared to the measured response to a 20-s stimulus for different percent of time spent for stimulation (ON) vs. fixation (OFF).

The implications of our preliminary results cited above could have significant impact on future applications and, more practically, experimental design constraints. First, the results suggest that BOLD contrast is highly sensitive to even subtle differences in neuronal activity in the first moments of activation. Thus, the information obtained from these "initial transient" maps might be much more meaningful neuronally, than the measures of steady state magnitude. Furthermore, if a linear relationship between neuronal activity over a population of neurons in a voxel and BOLD signal is established, then the implications for interpretation of subtle modulations of the BOLD signal will be highly significant at a functional level. Practically, the sensitivity of the deconvolved response to duty cycle is an important piece of information to keep in mind when comparing activation across several conditions from similar voxels. It is necessary to keep the relative duty cycle the same for all conditions to be able to correctly infer differences in amplitude to reflect differences in neuronal activity as they relate to the task and not the task duty cycle.

A obvious missing component to all of these studies is a more direct measure of neuronal activity with which to compare. While we are planning to collaborate with groups doing work on primates to obtain electrophysiological measures corresponding to these stimuli. We also are looking into complementing the above studies in humans through performance of identical experiments with MEG and EEG to further verify the neuronal responses. While these measures also involve a degree of uncertainty in regard to spatial location, their dynamics can more directly infer neuronal activity dynamics than can measured hemodynamic changes.

1C-3. Sensitivity of BOLD contrast to neuronal firing rate vs. number of active neurons

An open question regarding BOLD contrast concerns the type of neuronal activity that it is sensitive to. Does it matter how neuronal activity is temporally and spatially integrated within a voxel in the time scale of the hemodynamic response? Given a constant integrated neuronal activity, do many neurons firing infrequently elicit a different BOLD. In this study, the central issue is not whether or not local field potentials or spiking influence BOLD changes. We assume that for these particular stimuli, changes in local field potentials and spiking rates that correspond to changes in the stimuli parameters are proportional to each other.

Some studies report linear increases in BOLD-signal in human MT (hMT+) with increasing stimulus coherence in random dot displays [23, 36] which is interpreted as evidence for a linear relationship between non-simultaneous measures of neuronal firing rate and hemodynamic changes [23]. Other studies, however, found higher activity in hMT+ in response to incoherent motion compared with coherent motion [37] or no difference at all [38].

To test how motion coherence modulates the BOLD response in hMT+ and other areas we used a blocked design fMRI study (3T GE Signa) in which subjects viewed a random dot display for 1s and decided whether the stimulus was moving to the left or to the right. Coherence varied randomly from block to block (0%, 6.4%, 12.8%, 25.6% and 51.2%). hMT+ was identified independently, Figure 8a, using a low contrast motion stimulus (LCMS). Shown in Figure 8b is the response magnitude from this region as a function of stimulus contrast. Note the non-monotonicity of the curve.

In a second blocked design fMRI experiment, we tested whether the non-monotonic shape of the BOLD response was due to attentional effects. In addition to the random dot stimulus, the letters L and T where flashed rapidly (5Hz) at fixation. Before each block the subjects were cued to either do the letter discrimination task (count the number of Ls or Ts, LETT) or the motion discrimination task (MOT). When subjects performed LETT the BOLD response in hMT+ was smaller than during MOT; the shape of the BOLD response as a

function of coherence, however, was U-shaped in both experiments. Thus it is unlikely that the non-monotonicity in the BOLD-response is due to attentional modulatory effects.

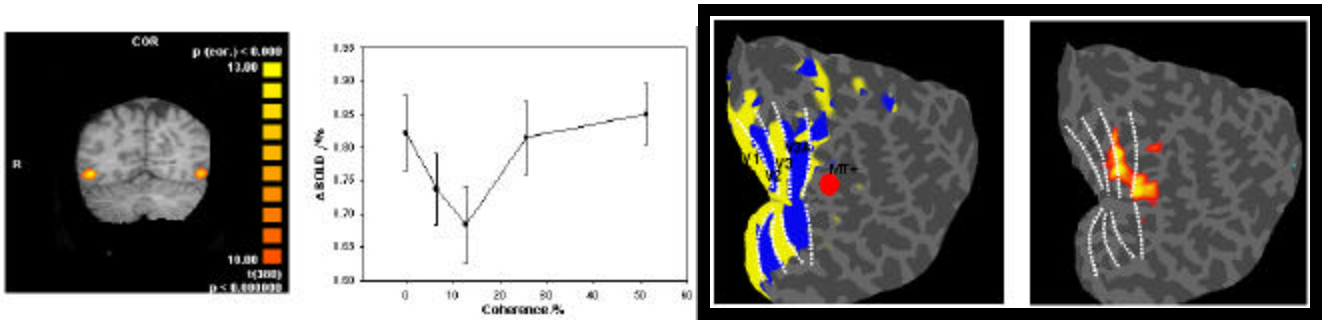

a. **b.** **c.**

Figure 8. a. hMT+ localized with a low-contrast moving stimulus. b. BOLD signal change in hMT+ as a function of coherence (N=6). Note the non-monotonicity of the curve. c. Retinotopic areas and result of group analysis using a U-shaped reference function displayed on the flattened occipital cortex of one subject. Note the main foci in V3/V3A and hMT+.

These data are consistent with a recent study reporting that in anesthetized monkeys BOLD signal varied non-monotonically as a function of noise in visual stimuli[39], supporting the view that BOLD-contrast measures a heterogeneous pooled neural response. According to this view, at 0% coherence (pure noise) many weakly activated neurons with different preferred directions would cause a similar summed BOLD response as few highly active neurons at 51.2% coherence tuned to that direction.

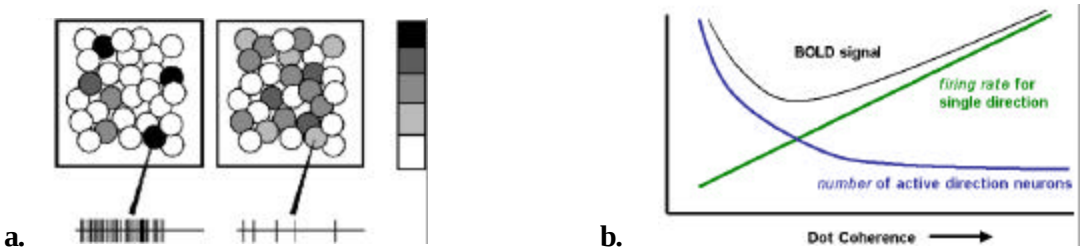

a. **b.**

Figure 9.a. Contribution of number of neurons firing and firing strength to summed population response (adopted from Rainer et al. 2001). B. Hypothesized component contributions to BOLD signal and their subsequent summation to produce the curve in Figure 8.

To test the this model directly, we are currently using motion stimuli with which we titrate separately the firing rate and the number of active neurons by parametric manipulations of the number of dots, their coherence, and velocity. According to this model, we predict that BOLD contrast change corresponding to changes in either firing rate or to the number of active neurons will be more rapid than the other, thus summing to cause the observed dip in BOLD response at 12% contrast.

1C-4. Use of multi-echo acquisition and velocity nulling to characterize vessel size and intravascular contribution.

Pulse sequence modulation, and therefore modulation of the sensitivity to components of the vasculature contributing to BOLD, is an useful method by which BOLD contrast can be better understood. Brain activation-induced signal changes arise from oxygenation-related modulation of magnetic field gradients in blood plasma surrounding intravascular red blood cells and extravascular gray matter and cerebrospinal fluid (CSF). The relative contributions of these vary on a voxel-wise basis as well as with MRI parameters that cause differential weighting to the components. Our goal is to first to map, at 3T, the relative CSF and intravascular contribution to BOLD contrast, then to construct methods to utilize this information to calibrate BOLD magnitude interpretation.

Three concepts are relevant to our hypothesis. First, diffusion weighting reduces signal from rapidly moving spins, such as extravascular CSF and intravascular blood. Deoxygenated blood has a higher transverse relaxation rate (R2*) than gray matter, whereas CSF has a lower R2*. Therefore, the change in R2* (either increasing or decreasing) with diffusion weighting will reveal, on a voxel-wise basis, whether more CSF or blood was removed. Second, the activation – induced ΔR2*/ΔR2 ratio is known to be positively correlated to the compartment size of the susceptibility perturber, with a smaller ratio for the small intravascular red blood cells and capillaries. Third, the amount of signal from CSF can be reduced by decreasing the TR.

Our hypothesis is that in voxels with a large contribution of the signal from intravascular blood, diffusion weighting will result in a decreased baseline R2* and an increase in the ΔR2*/ΔR2 ratio. Conversely, in voxels with a larger contribution of signal from extravascular CSF, diffusion weighting will result in an increased baseline R2* and a decrease in the ΔR2*/ΔR2 ratio. Shortening the TR will result in less signal from CSF, and hence a lower increase in baseline R2*.

Our preliminary results, shown in Figure 10, demonstrate that voxels with the largest baseline ΔR2* have the highest ΔR2*/ΔR2 ratio, supporting the fact that the largest signal changes arise from larger vessels. These voxels are also affected most by diffusion weighting, but the positive correlation between ΔR2* and the ΔR2*/ΔR2 ratio remains. The baseline R2* in most voxels is increased with diffusion weighting, implying that extravascular CSF is a significant contributor to the BOLD signal. This change is reduced at a shorter TR, likely due to reduced contribution of CSF to the signal. Voxels that show the greatest change in ΔR2* with decreasing TR generally show an increase in the baseline R2* with diffusion weighting, supporting the hypothesis that these areas are highly weighted by CSF.

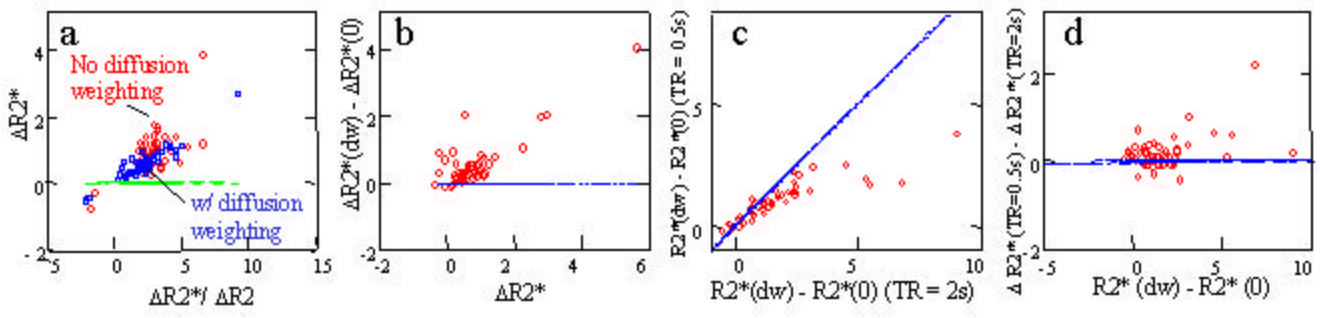

Figure 10: a) Activation-induced change in transverse relaxation rate (DR2*) with and without diffusion weighting (DW), compared to the DR2*/DR2 ratio, an indicator of compartment size; b) The change in DR2* when DW is applied compared to the magnitude of activation, DR2*; c) The change in baseline R2* when DW for a short TR compared to a longer TR; d) The change in DR2* when TR is changed vs. the change in baseline R2* when DW is applied.

The use and interpretation of spin-echo sequences for measuring ΔR2 has raised the question of the origin of functional contrast in spin-echo sequences. While it is assumed that spin-echo functional images reflect purely changes in R2, recent studies have suggested that a component of the observed functional signals may be due to proton density changes [40]. Simulations we have performed further indicate that the signal is partly R2*-weighted due to the long readout time associated with echo-planar sequences. The magnitude of this effect will be estimated using a phantom with a current carrying wire to simulate the susceptibility changes during functional activation. These experiments are currently underway.

In order to improve characterization of the sources of signal changes when using SE sequences, we implemented a simultaneous gradient-echo/spin-echo (GE/SE) technique with the same readout waveforms as EPI but using multi-shot phase-encoding steps instead of single-shot blipped gradients), here termed Echo Relaxation Imaging (ERI). For each excitation, a total of 64 echoes from GE and 64 echoes from SE were acquired at the same phase encoding step. This enables a fine sampling of the relaxation curve during the free induction decay and around the SE peak, allowing an accurate measure of the T2* and T2 changes during a motor task paradigm. ERI allows us to investigate activation-induced T2*, T2', and T2 changes in the cortex without confounding effects of a long readout window (and intermixed T2' effects) associated with EPI.

Since blood T2* becomes shorter at high field strength, part of the signal sampling using standard SE EPI is likely to happen during T2* decay on either or both sides of the SE peak. It is possible that part of the typical SE BOLD contrast is coming from the T2' rather than T2 changes. The results from these ongoing studies may impact the assessment of SE-EPI sequences to localize capillary based activation.

Theme 2: Methodology

2A. Introduction: What is the role of methodology advancement?

Methodology advancement is the link between advances in fMRI interpretation and their relevant applications. Since methodological issues in fMRI do not fall easily into the framework of hypothesis driven questions, they are commonly overlooked. While the immediate scientific focus of UFIM is directed towards understanding the relationship between neuronal activity and measured signal changes, and the overall goal of UFIM is understanding human brain organization and function, a primary effort of UFIM is the development of methods that aid neuroscientists and clinicians toward more effectively utilizing the potential of fMRI. Because of the rapid changes that fMRI is still undergoing, and will continue to undergo for at least the next decade, methodology advancement in itself is a critical component of any complete fMRI research program. I believe that most substantive methodological advancements also take place with the interpretation issues and neuroscience questions firmly in mind.

The following research summary consists primarily of methods that can be immediately utilized by the fMRI community. These include methods that extract useful components of the hemodynamic response, enhance experimental design, aid in data interpretation, and help to determine what scanning parameters to use.

2B. Progress Report

2B-1. Extraction of hemodynamic latency and width information

In BOLD contrast based fMRI, the hemodynamic response *amplitude* is most commonly used to characterize functional activation. Sole use of amplitude as a dependent measure limits interpretation to comparison of relative levels of activity between tasks (e.g. is area "x" activated more for task A or task B ?). In the past few years event-related designs and analysis procedures have allowed for a more precise estimate of the BOLD impulse response function (IRF) to event classes. The development of event-related designs has also led the way to unique methods for extracting information from the BOLD response including sorting BOLD responses with regard to behavioral performance, mental chronometry using hemodynamic delay estimates to infer neural information flow, and estimates of hemodynamic width to infer areas with increased processing demands or processing time. Increasing our ability to accurately map all the relevant characteristics of the BOLD response will help us better understand the complex relationship between neuronal activity and BOLD responses, thereby allowing investigators to ask more sophisticated questions. For example, simultaneous measures of hemodynamic delay and width would aid in resolving mental chronometry and relative processing time, thereby resulting in more detailed investigation of cognitive neuroscience models.

In this work, a method for estimating both delay and width in addition to amplitude was developed by Dr. Ziad Saad in close collaboration with UFIM. The direct application of this method is described in Theme 4B-1[41].

The method developed to estimate width and latency information independently is as follows (see Figure 11). The Full Model F-statistic from the deconvolution procedure was used to restrict the hemodynamic characterization analyses to only those voxels that were significantly activated. For each subject, the deconvolved IRFs of activated voxels were upsampled by a factor of 10 and modeled as a convolution of a Gamma Variate function with a Heavyside function of variable delay and width. To account for subject-to-subject variability in the average IRF, separate estimates of the Gamma Variate function parameters were obtained for each subject by fitting the function to the average IRF. Amplitude, delay and width of the IRF of

each activated voxel were obtained by fitting the IRF model to the empirical IRF estimate. This non-linear fitting was performed using the Nelder-Mead simplex method implemented in Matlab.

To improve the convergence of the algorithm to a meaningful solution, the fit was computed using a set of initial values for delay and width ranging in 0.5 s increments between 0 and 4. The parameter combination resulting in the best fit was then used as a center for another set of delay and width values covering a range of 1 s in finer increments of 0.2 s. The result of the second pass provided the final estimate of delay and width for a particular voxel's IRF. The importance of this technique is that it provides a new class of information (i.e. relative timing), by which upstream processing, processing bottlenecks, and downstream processing can be characterized with an accuracy on the order of 100 ms.

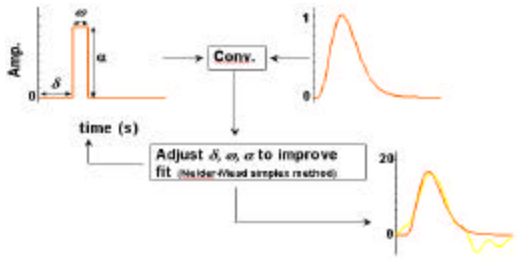

Figure 11: Illustration of the Nelder-Mead simplex method by which the independent estimators of delay, w?width, a, and amplitude, d, are mapped. With a TR of 1 sec, and with the assumption of an approximate shape of the hemodynamic IRF resembling a Gamma Variate function, these width and delay estimates may be obtained with an accuracy on the order of 100 ms.

2B-2. Choosing the optimal stimulus timing - detection vs. estimation

Functional MRI relies on the detection of relatively small (1-5%) signal changes over time. Because of this, there is interest in designing stimulus paradigms that maximize the efficiency of estimating the parameter of interest, such as the amplitude of activation, the shape of the hemodynamic response, or the latency of the response onset. Studies have proposed stimulus timings to optimize either the estimation of the IRF or the detection of signal changes [42-44].

Using a series of simulations, we demonstrated that estimation of the IRF and detection of the signal assuming a predetermined response are fundamentally different, and are optimized by different stimulus timings and distributions [45]. These simulations, shown in Figure 12, indicate that *estimation* of the hemodynamic IRF is optimized when stimuli are frequently alternated between task and control states, with shorter inter-stimulus intervals and stimulus durations, whereas the *detection* of activated areas is optimized by blocked designs.

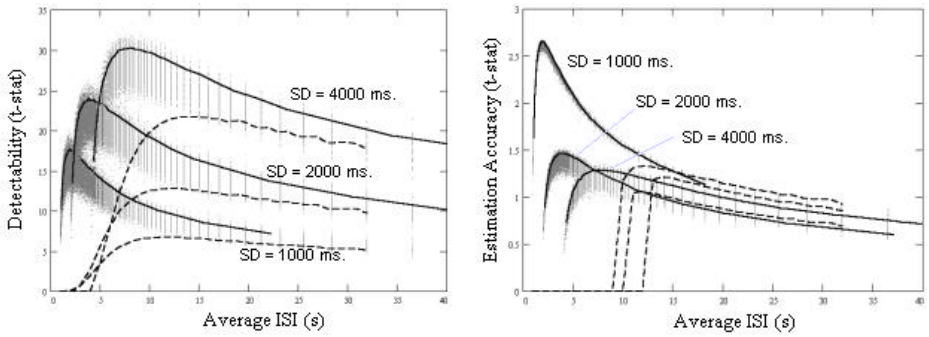

a b.

Figure 12: a. Detectability and b. Estimation accuracy vs. average interstimulus interval (ISI) for stimuli with varying ISI (points and solid lines) and constant ISI (dashed lines) for 3 different minimum stimulus durations: 1000 ms, 20000 ms, and 4000 ms. Each point is the detectability and estimation accuracy for one time series. The line represents the detectability and estimation accuracy 5% from the maximum. Stimulus patterns with larger minimum stimulus durations (SD) are more similar to blocked designs, varying more slowly between task and control states. Detectability increases with larger minimum stimulus durations.

2C. Current and Future Experiments

2C-1. Optimization for latency detection.

An additional goal for certain fMRI studies is the estimation of the latency of the BOLD response. This estimation relies heavily on the transitions in the measured signal between the task and control states. It is therefore expected that stimuli with more frequent transitions and hence shorter block lengths will allow a better estimation of the response latency. A short stimulus duration, however, results in a smaller response, and a brief control period does not allow full recovery of the signal to baseline. These two opposite effects suggest that there is an optimal intermediate stimulus block duration.

Results from simulations, shown in Figure 13, indicate that for a varying interstimulus interval (ISI), the most efficient design consists of a stimulus with exactly half of the time spent in either the task or control period, at an average ISI of 2 s for a 1 s duration stimulus. For a constant ISI, the minimum occurs at 8 s. The optimal block duration is approximately 4-6 s for both a constant and varying ISI.

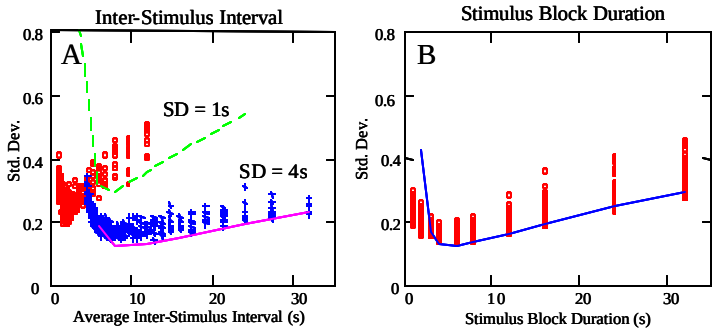

Figure 13: a: Standard deviation of latency estimate for varying inter-stimulus intervals, at a stimulus duration of 1s (o) or 4s (+). Lines represent ISIs constant in time. b: Standard deviation of latency estimate for different stimulus block durations and an equal amount of time in stimulus and control states. Circles: varying ISI, Line: constant block duration and ISI.

Since the accuracy of estimating a particular delay generally increases with the square root of the number of samples, the results suggest that 3.5 runs of 192 s in duration (at a TR of 1s) are needed in order to accurately detect a latency difference of only 100 ms ($p<0.05$). The choice of the proper stimulus design has a large impact on this, with less optimal designs possibly resulting in 2-3 times the standard deviation, and therefore requiring many more samples for accurate latency determination. We plan to verify these results empirically.

2C-2. Optimization for tasks involving subject motion.

The assessment of cortical activity by fMRI in the presence of overt word production or other types of necessary task-related motion is of great interest and importance, as it would increase the possible fMRI experiments, but it has been severely impeded by artifactual signal changes arising from subject motion inherently coupled with the subject's speech. Recent studies have demonstrated that these artifacts can be reduced by using an event related imaging paradigm (ER-fMRI) with long ISI. This relatively slow stimulation rate, however, requires long scan times and is not optimal for many neuropsychological tests. The goal of our study was to develop and test a technique by which fMRI activation maps can be acquired during more frequent overt speech.

In a blocked design paradigm artifacts arise because motion induced signal changes are strongly correlated with the expected hemodynamic response. These artifacts are reduced in ER-fMRI with long ISIs since the intrinsic hemodynamic delay causes the motion induced signal changes to occur prior to the BOLD response. By varying the ISI, stimulus paradigms can be specifically designed to occur more frequently and to minimally correlate with the resulting BOLD response. Using a variable ISI has the additional advantage over constant ISI paradigms in regard to statistical power.

The simulation results, shown in Figure 14, demonstrate the balance between motion sensitivity (sensitivity to rapid signal changes) and hemodynamic sensitivity (slow changes). The goal is to maximize the latter while keeping the former at or near zero. As can be seen, similar optimal results are seen for blocked design alternating 10 s on and 10 s off and for varying ISIs having a minimum SD of 5 sec. Again, we plan to verify these results empirically.

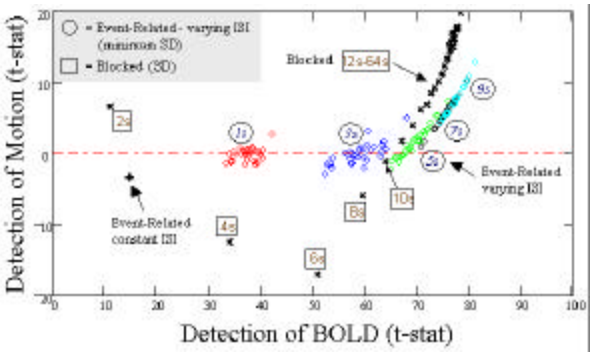

Figure 14: Simulations of detection of BOLD response vs. sensitivity to motion for constant ISI (+), varying ISI (o), and blocked design (x) at various duty cycles and average ISI values. The optimal stimuli timings maximize detection of BOLD while minimizing detection of motion. As shown, for blocked designs, this occurs at 10 s on, 10 s off. For constant ISI event-related fMRI, this occurs at an ISI of about 12 s. For jittered ISI event-related fMRI, this occurs at an average ISI of about 5 s.

2C-3. Choosing the optimal spatial resolution

The goal of this work is to give a clear framework by which to decide on the necessary sensitivity and possible resolution at which to carry out an fMRI experiment. Our focus is on the relationship between image signal to noise ratio (ISN) and time series stability (here termed temporal signal to noise ratio (TSN)). TSN is a key determinant in fMRI detection power. Because of physiologic fluctuations (PF), (i.e. originating from respiration and pulsations at the cardiac frequency), that are manifest over time but not on the time scale of each single shot echo planar image (about 40 ms), gains in ISN do not necessarily translate into gains in TSN [47]. PF sets an upper limit to the possible gains in TSN with improvements in ISN. While effort has met with success in reducing time series fluctuations in multi-shot imaging [46], these effects are difficult to filter in single shot imaging at a constant TR because of their broadband frequency characteristics. This work therefore focuses on understanding the characteristics of typical uncorrected signal shot image time series. As higher field strength systems and higher sensitivity surface coil arrays become more ubiquitous, the issue of how to best make use of increased ISN is of increasing importance. Our hypothesis is that the primary impact of increased ISN is to allow fMRI to be carried out at higher resolution – where ISN approximately matches TSN or is significantly lower than the limit set by PF. We roughly define "optimal resolution" as the resolution where TSN begins to approach this physiological limit – where further increases in ISN give highly diminishing gains in TSN.

The relationship of ISN and TSN vs. voxel volume was experimentally determined with multiple-resolution fMRI studies performed at 3T, using a quadrature transmit/receive head coil (low ISN) and a 10" receive only surface coil (high ISN). The spatial resolution was modulated by field of view (FOV) stepping (14 cm, 16 cm, 18 cm, 20 cm, 22 cm, 24 cm, 36 cm, 48 cm, 60 cm). TE: 30 ms, TR: 1 s, BW: 125.0 kHz, flip angle: 90 deg. Thermal noise measurements were obtained using a flip angle of 0 deg. At higher resolutions, both ISN and TSN are reduced well below the upper TSN limit, so therefore have similar values since the contribution of PF is reduced. The gain in coil sensitivity is essentially lost at larger voxel volumes, but is manifest at smaller volumes where the ISN dominates. However, the higher the overall ISN, the higher the resolution is at which this plateau is reached. One further consideration that remains to be characterized completely is that at higher resolutions, as voxel volume approximates the size of the activating unit, the functional contrast will increase, therefore reducing the optimal voxel volume further.

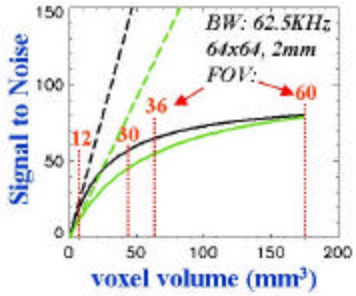

Figure 15 Image and Temporal Signal to Noise (ISN and TSN respectively) vs. voxel volume for surface coil (gray line) and head coil (green line). Straight lines are ISN (signal at 90 deg. flip angle / signal at 0 deg. flip angle). Dotted lines are ISN (signal at 90 deg flip angle / standard deviation of signal measured over time) and solid lines are TSN. Here, the upper limit in TSN is approximately 80.

The optimal spatial resolution occurs below where TSN begins to approaches a plateau, as larger voxel volumes will not further enhance detectability. It is important to keep in mind as well that imaging at a higher resolution

than "optimal" is of course necessary with almost any currently achievable ISN in order to image such structures as ocular dominance columns. A formalism for the relationships presented are being developed such that an "optimal resolution" can be calculated for any sensitivity, given the ISN, TSN and the expected signal change.

Ongoing research is currently being carried out to determine a robust method to map the optimal resolution on a voxel-wise basis. Investigation into the *relative* sources of PF is also being conducted. One idea for extracting PF is by the use of two receiver coils that receive signal from identical areas. Comparison of the time series signal will allow separation of thermal noise from PF based on the understanding that thermal noise (between two coils) is completely uncorrelated over time but the PF are not. These investigations may lead to methods for complete removal of all PF from fMRI time series.

Theme 3: Technology

3A. Introduction: What is the focus from a technology standpoint?

UFIM has worked synergistically with FMRIF over the past four years to develop technology aimed at enhancing the ability to ask fundamental questions related to Theme 1 and towards immediate utilization in Theme 4. In addition, a brain imaging technology advancement goal of UFIM that does not fall into either of these categories has been the exploration of the feasibility of directly measuring magnetic field changes induced directly by neuronal currents, bypassing hemodynamic contrast altogether.

At the core of the technology development is improvement of sensitivity and improvement in specificity. Pulse sequence development has taken place, resulting in such sequences as ERI, mentioned in Theme 1C-4. Hardware development has resulted in a 16 receiver coil arrays coupled with 16 independent channels at 3T. This powerful coil and receiver setup, the first of its kind in the world, as been accomplished by Jerzy Bodurka (FMRIF) in collaboration with Jeff Duyn and his Section on Advanced MRI (SAMRI) in NINDS. I am also involved with the project in regard to carrying out studies to quantify the gains achieved by these advancements. The benefits of this technology are only beginning to be realized. Pulse sequences able to image at high resolution with a high degree of temporal stability, requiring the use of advanced phase correction methods, are currently being developed. Also, parallel imaging techniques, making direct use of this 16 channel array, have been developed by SAMRI. UFIM and FMRIF are currently programming robust reconstruction methods for parallel imaging to be used by the wider NIH community. With these improvements taking shape, within the next 4 years, it will be routine for whole brain functional MRI to take place using submillimeter voxel sizes while maintaining a sensitivity high enough to detect 1% signal changes.

3B. Progress Report

3B-1: Neuronal Current Imaging: model calculations and phantom results.

Functional MRI is based on the sensitivity of MRI to oxygenation, flow, and perfusion changes concomitant with an increase in brain activation. The spatial and temporal resolution of fMRI are limited by cerebral neuronal-hemodynamic coupling precision, rather than physical limitations of the imaging methodology. Magnetoencephalography (MEG) and electroencephalography (EEG) allow measurement of brain electric activity with a temporal resolution on the order of milliseconds but with lower spatial resolution (1-3). Significant effort has been made to combine information from these different modalities in order to obtain high spatial and temporal resolution maps of brain activation. An ultimate goal is the direct mapping of these dipole sources. We introduce and outline the feasibility of an MRI–based method to directly detect and map transient magnetic field changes corresponding to synchronous neuronal firing[48]. The weak ionic currents (on the order of nA) resulting from brain activity induce subtle and transient magnetic flux density (ΔB) changes, depending on their temporal and spatial coherence. The component of these fields that is parallel to the main magnetic field (referred to as ΔB_0) alters the magnetic phase of surrounding water protons and thus influences the phase and/or magnitude of the MRI signal – depending on the size and geometry of the synchronous current sources.

Evoked or spontaneous magnetic field changes measured on the scalp by MEG (the measurement distance is about 2-4 cm away from the current source) are on the order of 10^{-12} (spontaneous) to 10^{-13} (evoked) Tesla. These fields primarily result from a synchronized activity of postsynaptic currents in a large number of the pyramidal neurons (50000 or more that occupy an area of a few mm^2) of the cortex[49].This spatial scale is approximately that of a typical MRI voxel. For visual/auditory stimulations, typical ΔB_0 peak values are in the order of ≈10-13 fT and lasting on the order of 100 ms. MEG data and calculations suggest that current sources causing these magnetic field changes, assuming an approximate MRI scale of 1-2 mm, could create ΔB changes near the source (approximately scaled as $(rMEG/rMRI)^2=10^3$) on the order of 10^{-9} to 10^{-10} Tesla

The primary motivations of this theme are a) to develop and demonstrate a new MRI-based methodology and a new class of an experimental paradigms for detection of ultra weak and transient magnetic field changes, and b) to determine if the physiologically-relevant transient fields (<100ms) in the order of 10^{-10} Tesla are detectable by MRI, c) to conduct in vitro feasibility studies and, finally, d) to conduct preliminary human experiments.

Because of the transient nature of targeted ultra weak magnetic fields it is necessary to develop completely new experimental strategies. A key element is the stimulus delivery system which provides high accuracy shot-to-shot synchronization with the MRI scanner. A confound is the large global magnetic field shifts that are induced by subject respiration. A proposed pulse sequence for this detection is a single-shot spin-echo (SE) echo-planar sequence (EPI) that selectively detects transient (< TE/2 = 50ms) changes in magnetic field and suppresses slow (>TE/2) magnetic field changes. The sensitivity of SE to transient magnetic field changes is based on the fact that the 180 pulse refocuses any changes that occur slowly (i.e. greater than 500 ms) over time while does not refocus changes that occur within 50 ms. These rapid changes therefore appear as either phase shifts or magnitude changes (depending on the geometry of the source of the change).

The method was tested on a phantom that contains wires in which current is precisely modulated. At present, with this method, magnetic field changes as small as 2×10^{-10} T (200pT) and lasting for 40 ms can be detected, as shown in Figure 16.

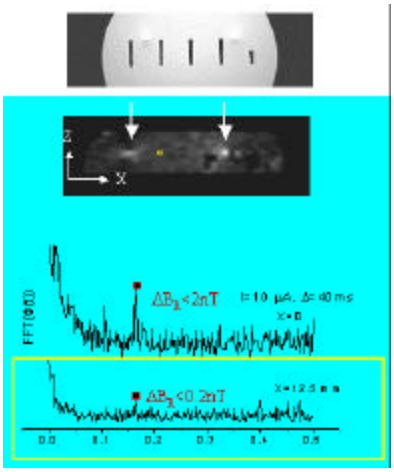

Figure 16: Current phantom results. The white arrows indicate wire positions. The middle panel shows FFT of the magnetic phase time course from a voxel containing the wire indicated by the left arrow. The bottom framed plot shows the FFT spectrum from a voxel 12.5 mm from the left wire (indicated by a rectangle). Within the voxel, which contains wire, the current-induced field shift is 2 nT. The field shift in the selected voxel at the distance of 12.5 mm from the left wire is calculated to be 0.2 nT or 200 pT. Such a field shift produced a well-resolved peak at the ON/OFF frequency (0.17 Hz). In vivo, uncertainties of neuronal activation timing and waveform shape, as well as physiologic fluctuations on the order of 10 nT will need to be overcome to detect activation-induced magnetic field changes in the human brain. A hope is that, at the "dipole" source, when using high enough resolution MRI, zero dipole cancellation takes place, therefore increasing the current and magnetic field changes beyond what has it has been theoretically calculated to be from inverse models of measured current on the scalp.

3C. Current and Future Experiments

3C-1. Neuronal Current Imaging: in vitro and human results.

To carry further the neuronal current experiment described above, we wished to determine if synchronous neuronal activity was detectable in vitro. An in-vitro model consisting of coronal sections of newborn-rat brains (in-plane: 0.3-1 mm^2, thickness: 60μm) was used to test the feasibility of the method. The slices contained cortical and basal ganglia tissue, which form a feedback system exhibiting spontaneous synchronized activity at

< 2Hz [50].This model is ideal as it contains active neuronal tissue and no blood flow or pulsations that may contribute to MRI signal changes.

Two data sets were acquired for each of the following states: active: spontaneous synchronized neuronal activity, inactive: neuronal activity terminated by injecting TTX (Tetrodotoxin: neuronal membrane sodium channel blocker). A high resolution fast spin-echo (FSE) image was used for localization. Power spectra (per voxel) were calculated form the resulting phase images and were analyzed with Principal Component Analysis. The dominant spectral components, i.e. with the highest variance (total 6), for both the active and inactive states were obtained for the culture (9 voxels encompassing the culture site, selected based on the FSE images) and CSF (for the remaining voxels containing only CSF, appx. 420). The dominant spectral components were compared between the active and inactive states, for both the culture and CSF locations. As shown in Figure 17, spectral peaks were attributed to neuronal current effects if and only if they were present in the culture location during the active state, and had achieved statistical significance over the noise level.

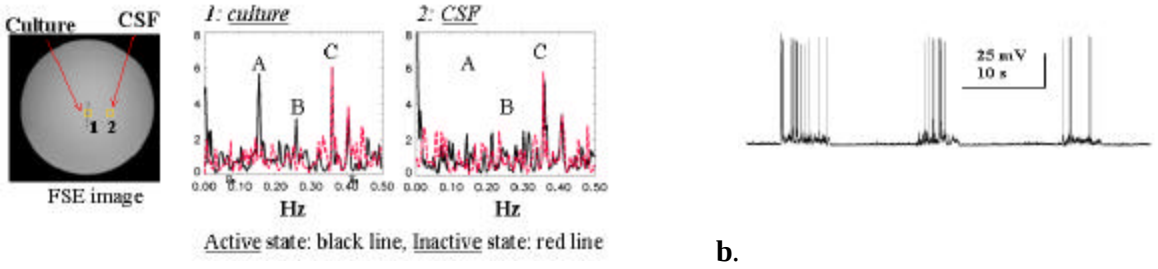

Figure 17: a. In vitro results: A and B: synchronous spiking activity of culture, C: scanner noise (cooling-pump). b. Typical spontaneous spiking temporal pattern arising from the culture.

MEG data suggest that magnetic fields from spontaneous activity (alpha rhythm, frequency range 8-12 Hz, central frequency around 10 Hz) are an order of magnitude greater then evoked fields. Therefore, we first conducted resting state experiments. We wished to confirm detection of alpha rhythms. We modulated alpha wave activity by having the subject either have their eyes opened or eyes closed for durations of 5 minutes at a time. Preliminary data (see Figure 18) shows normalized power spectra images and spectra from a marked voxel (black box) at 0.12 Hz, (hypothesized to be the aliased alpha rhythm frequency) for both eyes closed and eyes open conditions.

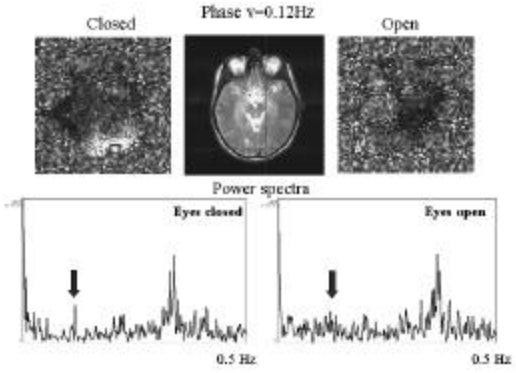

Figure 18: Preliminary human data showing the power spectrum of MRI phase during open and closed eyes conditions. The images show an area of increased power in the region commonly associated with alpha wave activity at what is presumed to be an aliased frequency of alpha wave activity manifest as a current induced phase shift.

The MRI sensitivity to a weak and transient signal induced by neuronal activation is primarily SNR limited but is also limited by uncertainty of the timing of evoked neuronal transients in the human brain. The MRI window with which to capture these transient effects is on the order of 50 ms so therefore needs to be precisely placed relative to evoked responses. We are developing rapid multi-echo pulse sequence strategies combined with tailored processing techniques that will allow us to capture the entire evoked transient response with MRI.

The combination of sensitivity improvements from 16 element surface coil arrays and 16 channel MRI receiver capabilities in combination with the increased signal to noise benefits of imaging at 7 Tesla – all being developed in close collaboration with the Section on Advanced MRI (SAMRI / NINDS) headed by Jeff Duyn - can greatly enhance MRI sensitivity to transient magnetic field changes of neuronal origin. We are also planning

to implement high resolution methodology in combination with PF reduction techniques (e.g. [46]) to further improve detection capability.

We are also planning the neuronal input more carefully. Currently, we are performing experiments involving driving the visual system with a sinusoidally alternating checkerboard stimulus - known to induce local field potential changes at precisely the same frequency. We plan to use this well-defined stimulus in conjunction with precise pulse sequence synchronization and processing methods designed to optimally extract these frequencies – if they are indeed extractable.

This is clearly a project that has a potentially important impact on functional imaging in general. It is also a project that has a significant chance of not succeeding since it may turn out that the necessary temporal sensitivity may be too low and/or the magnitude and extent of the current induced field changes may be underestimated. At this stage in experimentation, this information (maximum achievable temporal sensitivity, magnitude of neuronally induced magnetic field changes, spatial scale of the field changes) are not fully characterized. As mentioned, advances will be made by increasing temporal sensitivity, improving the precision of neuronal activation, and improving the efficiency of the post processing methods. Lastly, confirming any demonstrated effects of neuronal current-induced changes in humans as completely separate from BOLD contrast is a non-trivial necessity. To do this will require careful modulation of pulse sequence and task timing such that BOLD contrast and transient neuronal current effects are differentially selected. I currently have two researchers, Jerzy Bodurka (collaborating from FMRIF) and Natalia Petridou, working on this project.

Theme 4: Applications

4A. Introduction: Carrying Themes 1 - 3 through to Theme 4.

Applications of fMRI that come out of UFIM are those that make the best possible use of the results of Themes 1 through 3 and the available technical expertise in UFIM and FMRIF. The questions here are not driven by the themes but rather use the outcomes of these themes and apply them to neuroscience questions.

As an example, the application in 4B-1 directly utilizes the techniques developed in 2B-1 and 2B-2 for paradigm design and processing. It also utilizes an understanding, derived from work in UFIM and elsewhere, that while the variability of the hemodynamic response over time *within each voxel* is small enough to reveal modulations (using a comparison tasks) in neuronal activation timing on the order of 100 ms, the spread in the hemodynamic response *across voxels* (4 s) does not allow for assessment of lexical processing streams (occurring on the order of a 100 ms) without a comparison task of a slightly modulated timing. The study described in 4B-1 is among the first to implement this strategy to reveal processing stream modulation.

The studies described below report novel findings primarily in lexical processing and in autonomic circuitry. The paradigms used in 4B-1 and 4C-2 have been guided directly by 2B-2. In addition, the hypothesis in 4C-2 is directly motivated by results from single unit recordings. In general, fMRI hypothesis driven by such findings are well constrained and will provide with an immediate advancement of the results of such physiologic data since the results provide information on wider spatial scale yet may be compared in similar regions with single unit recordings that have been established. Lastly, an ongoing effort of UFIM has been to make maximal use of the entire time course of data, and specifically towards extraction of relevant neuronal information from the temporal fluctuations. The continued development and use of simultaneous measures of physiologic state and performance as regressors is a primary focus of UFIM and a central point of the collaborations with LBC and the rest of the NIH.

4B. Progress Report

4B-1. Dissection of lexical processing streams using task modulation combined with latency, width, and magnitude measures.

The aim of this investigation was to determine whether a voxel-wise characterization of the hemodynamic response width, delay and amplitude would aid in attaching neuroanatomical markers to the cognitive processes of single words. The completed study [41] integrated results from Themes 1 and 2 to address sensitivity of fMRI for detecting regions involved in prolonged neuronal processing and automaticity of language processing. In this study, subjects performed a lexical decision task using word and non-word stimuli rotated 0, 60, or 120 degrees. Reaction times for these tasks are shown in Figure 19a.

Increased reaction time during a lexical decision for a nonword reflects extended processing in some component of the semantic-lexical processing network. We hypothesize that this reaction time delay is manifest as a wider hemodynamic response. Additionally, as stimulus rotation was proposed to result in an overall delay in language processing, we predicted a larger hemodynamic delay to be present in all language areas not involved in perspective change when the rotated stimuli are presented. Averaged hemodynamic response functions (HRF's) for each condition were fit to a Gamma-variate function convolved with a Heavyside function of varying onset and duration to estimate each voxel's activation delay and width (as described in 2B-1).

Figure 19b depicts averaged amplitude, delay and width difference group maps for the Lexical main effect (word vs. non-word) and Figure 19c depicts the same for the Rotation main effect (no rotation vs. either 60 degree or 120 degree rotation). Consistent with previous fMRI studies of lexical processing, subjects showed magnitude differences between words and non-words in language areas attributed to orthographic, phonological, semantic and post-lexical processing including fusiform gyrus, lingual gyrus, middle temporal gyrus, precuneus, superior temporal gyrus, middle and inferior frontal gyrus.

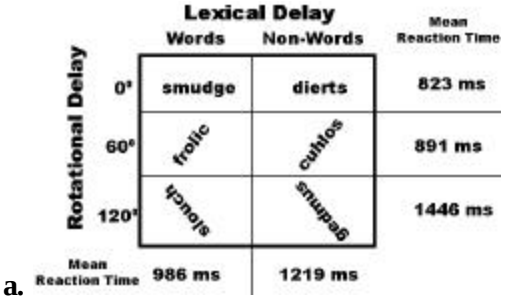

a.

Figure 19.a. Mean reaction time for each condition. b. Warm colors (Red / yellow) are areas where Words > Non-words. Cool colors (blues) are areas where Non-words > Words. The left hemisphere is toward the left margin. c. Warm colors (Red / yellow) are areas where Non-rotated stimuli > Rotated. Cool colors (blues) are areas where Rotated stimuli > Non-rotated. The left hemisphere is toward the left margin.

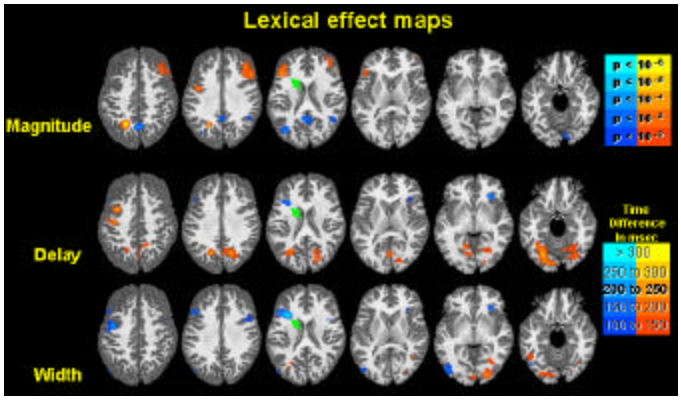

b

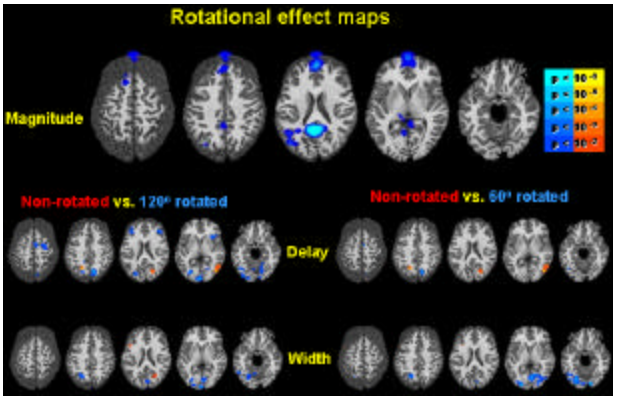

c

Left inferior frontal gyrus showed both a delayed onset to rotated stimuli ($p < 0.001$) and a width difference between HRFs for words and non-words ($p < 0.05$), suggesting that processing was prolonged in this region during the lexical decision component of the task and delayed when stimuli were rotated. Averaged time series obtained in the left inferior frontal gyrus are presented in Figure 20 as support for both the delay and width estimates. The middle temporal gyrus had three functionally dissociable regions. The superior regions showed

widening of the hemodynamic response to non-words, whereas a more ventral region showed no differential widths between stimuli but rather showed a delayed onset time for stimuli rotated. The anterior left middle temporal gyrus showed delayed responses to words relative to non-words but had no differential effects of stimulus rotation. The averaged HRFs in Figure 20 are representative of anterior middle temporal gyrus language areas. Differential responses in the middle temporal gyrus suggest diverse functional roles within this region during lexical access. Overall, these results suggest that phonological routes but not semantic routes to the lexicon can proceed regardless of stimulus orientation and that processing delays to non-words involve prolonged processing in the inferior frontal gyrus (IFG).

The design and analysis technique presented in the present study yielded insight into the cognitive systems involved in single word processing. BOLD amplitude differences between words and non-words have shown that the IFG is "more" active for non-words; however, magnitude cannot distinguish among several possible differences between the HRFs of words and non-words. The present study demonstrates that combinatory measurement of magnitude, delay and width can further interpretability of activations in standard fMRI activation maps. Stimulus estimates of delay provide information regarding the stream that processing may take and width estimates provide a sketch of areas that have prolonged processing demands put upon it. However, variability in brain vasculature between regions and even between voxels demands that each of these measures be standardized or calibrated. This study shows that appropriate task comparisons can produce difference maps that standardize the delay and width measures between voxels allow for more quantitative mental chronometric maps, adding a new dimension to the utility of fMRI.

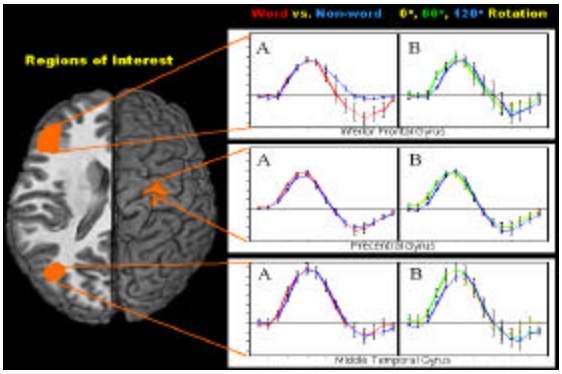

Figure 20. Graphs depicting the estimated Impulse Response Functions for both the lexical (words vs. non-words) and rotation effects (degree of rotation). Error bars represent the standard error of the mean and the left hemisphere is toward the left margin.

4B-2. Extraction of neural correlates of autonomic activity using simultaneous skin conductance measures.

Another application that directly follows from the previously mentioned themes of Interpretation and Method development is that involving simultaneous measures of skin conductance during fMRI time series collection. It is understood that the fluctuations in the time series contain not only random thermal noise but also information about resting state and spontaneously changing physiologic and neuronal processes. We used this knowledge combined with simultaneous independent measures of skin conductance to extract those fluctuations that show correlation with skin conductance, thereby deriving functional maps of baseline autonomic processes[51] .

In the present study, the network associated with skin conductance responses (SCR), was shown to be "spontaneously" activated during three different cognitive states: a gambling task, a working memory task, and resting state. SCR data were simultaneously collected during the scanning process. Six subjects were scanned at 1.5 T during all three states, and one subject was scanned at 3 T during the resting state only. SCR data were used as a reference function for correlation analysis with the fMRI time series during each of the three tasks (gambling, working memory, and rest). SCR changes were evident during all three tasks. SCR activity was not observed to be specifically related to reward-based decisions in the gambling task. Correlation of the fMRI time series directly with the SCR data revealed a consistent set of activated regions. The pattern of these regions showing correlation with the SCR appeared independent of the cognitive state. Further, the subject scanned only at rest (without the possible confound of task-related carryover activity) replicated the findings in the original six subjects. The SCR– correlated activity during rest is shown in Figure 21. From these data, SCR appears to be

a marker of a network that is active during, but independent of, the task being studied. These regions include the thalamus, cerebellum, cingulate, ventromedial prefrontal, and inferior parietal cortices.

The use of simultaneously measured behavioral/autonomic information as a regressor for the analysis of time series data is an important methodological development in fMRI in that it accomplishes the power of parametric manipulation but with the flexibility of allowing independent measure to fluctuate spontaneously from moment to moment.

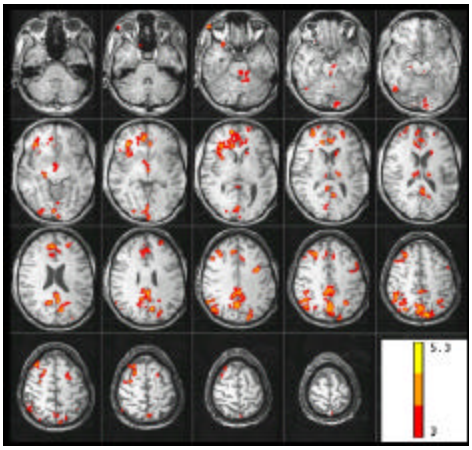

Figure 21. Regions of activity that correlated with SCR in a single subject during the resting state. The study was obtained from a single 15 minutes run in which the subject was lying with eyes closed while skin conductance was being recorded. Because SCR has similar dynamic characteristics as BOLD contrast, no smoothing or shifting was necessary. SCR data was down sampled to the TF and the correlation coefficient was recorded. From top to bottom is shown a series of axial images from the cerebellum to the apex. The Z-scores are represented by the color scale to the right.

4C. Current and Future Experiments

4C-1. Functional MRI of conditioned, unconditioned, orienting, and non-specific skin conductance responses during Pavlovian fear conditioning

In this preliminary ongoing work, we expand on what was presented in 4B-2. Skin conductance is a measure of autonomic arousal that is influenced by a number of distinct cognitive processes that are important to differentiate. For example, one concern with the use of autonomic measures in Pavlovian conditioning involves differentiating learning-related changes from changes due to orientation, pseudoconditioning, and sensitization. Electrodermal activity is sensitive to threat, stress, and novelty. Since each of these factors are present in an experimental situation, large orienting responses should be expected at the beginning of the conditioning session. As the session progresses, orienting responses habituate, and the effects of conditioning must be compared to decreasing orienting responses. By using two stimuli that initially produce similar autonomic responses, and pairing one (CS+), but not the other (CS-) with an unconditioned stimulus (UCS), and then comparing the two stimuli at the end of training, the observed differences should be due to learning the conditioned association. Conditioning would then be demonstrated by greater responses to the CS+ compared to the CS-. One conceptualization of autonomic responding is that orienting responses are elicited by novelty, while conditioned responses are evoked by anticipation of the UCS. Therefore, It is likely that the neural processes associated with orienting are different from those of conditioned autonomic responses during Pavlovian fear conditioning. However, an alternative theory is that conditioned responses (CRs) are simply orienting responses (ORs) that have been maintained by repeated pairing of the CS+ and UCS. Although these processes likely share a common neural network that controls general SCR, unique brain structures may differentially modulate the generation of orienting and conditioned SCRs.. For instance, the amygdala appears to contribute to the production of conditioned and unconditioned SCRs, but this region's role in the generation of SCRs related to other processes such as orienting remains unclear.

The CR and UCR likely rely on many of the same structures, and given the resolution limits with our imaging parameters we may not find differences between the structures supporting these 2 response types. For example, we are unlikely to be able to separate out subnuclei of the amygdala. However, to the degree that anticipation of the UCS influences CR production, we should expect to find differential brain activation since the UCR itself should not include cognitive process like anticipation. Its more likely that we will find differences between OR,

CR, and non-specific responses(NSR). Reasons for this include possible differences in "external" versus "internal" generation of these responses. The OR and CR are by definition elicited by CS presentations, while the NSR is elicited by factors not under direct experimenter control. For example, NSRs could be due to thoughts the subject has about issue not related to the study such as plans for later in the day.

Skin conductance is only one of many useful indices of autonomic function. Others include, but are not limited to measures of respiration, skin temperature, muscle tension, cardiac function, and pupilary dilation. These measures show differences in the onset and duration of responses. For example, changes in muscle tension as measured with electromyography (EMG) can occur very quickly, while alterations in skin temperature tend to occur more slowly. Further, the degree of volitional control individuals maintain over these functions can vary. For instance, individuals can easily modulate their respiration rate, while volitional control over skin conductance measures is much more difficult.

The present study uses a Pavlovian fear conditioning procedure to elicit orienting, conditioned, unconditioned, and non-specific skin conductance responses measured concurrently with whole brain fMRI.. Participants were presented a 10 s pure tone (CS+) that co-terminated with a 500 ms loud white-noise (UCS), a 10 s pure tone alone (CS-), and non-repeating noises (Novel) consisting of tone sweeps, whistles, and bursts of complex sounds. Stimuli were separated by a 20 s inter-trial interval (ITI). SCR that occurred during the 10 s following onset of the CS+, UCS, and CS-/Novel stimuli were classified as conditioned, unconditioned, and orienting responses respectively. SCR produced during the ITI that were not elicited by these stimuli were classified as non-specific responses.

Multiple linear regression using the hypothesized evoked hemodynamic response for conditioned, unconditioned, orienting, and non-specific responses was used to identify active brain regions. For all SCR types, significant activation was observed within a number of cortical and subcortical regions including the cingulate, thalamus, insula, cerebellum, and prefrontal cortex. Differential event-related activity was observed within the amygdala, insula, parietal cortex, and parahippocampal regions that reflected specific SCR types. These data suggest that a basic neural circuit supports the production of SCR, and that additional brain regions are recruited to modulate these responses by task dependent cognitive processes. The use of behavioral binning and simultaneous SCR measures have allowed us to further delineate processing specific and general networks associated with SCR changes over time

4C-2. Neural correlates of perceptual decision-making

Decision-making is one component in a heterogeneous group of higher order cognitive processes termed executive functions. Executive dysfunctions can be caused by a broad range of brain disorders. Available neuropschychological tests for the diagnosis of executive dysfunctions have poor specificity and sensitivity, making the early and differential diagnosis difficult. Thus executive dysfunctions are often underdiagnosed. The development of improved diagnostic and therapeutic approaches requires better understanding of these higher cognitive functions. The goal of the present projects is therefore to delineate upon which functional architecture and which neuronal mechanisms decision-making processes in the intact human brain rely.

Based on the findings from single-unit recording studies in monkeys, Gold & Shadlen have proposed a model for the perceptual decision-making process. According to the model the brain can form a categorical decision by integrating the difference in spike rates from two pools of neurons (“neuron/antineuron” pair) [52]. In a direction-discrimination task (up/down) a decision-variable can be computed by taking the difference between the neural responses of upward-sensitive and downward-sensitive neurons [53]. In an event-related fMRI study we tested whether there is evidence for a similar mechanism during human perceptual decision-making. We used a face-house discrimination task because pools of neurons that respond more to faces than to houses and vice-versa can be identified reliably with fMRI in the human brain. In a behavioral pilot study with phase scrambled images (see Figure 22B) of faces and houses, subjects decided whether an image presented on a screen was a face or a house. The behavioral pilot study showed that images of faces and houses with about 55% phase coherence were identified correctly with 82% probability (see Figure 22A).

In the event-related fMRI experiment we used four classes of stimuli. Images of faces and houses with high (percent correct above 95%) and low (corresponding to the 82%-threshold) phase coherence, respectively, were

shown on a screen for 1 s and subjects responded with a button press after a forced delay. To define the two pools of neurons representing the evidence for the two alternative categories (face/house), we identified fusiform ('FFA') and parahippocampal areas ('PPA') that responded most to faces and houses, respectively in each subject. We then averaged the BOLD-signal time courses within FFA and PPA, and computed the absolute value of the difference between the signal in FFA and PPA. In a second step, the resulting time course ('|FFA-PPA|') was used as an additional regressor. Within the regions that showed a main effect for higher phase coherence independent of category, the following regions covaried significantly with |FFA-PPA|: bilateral middle frontal gyrus (BA8/9, see Figures 22 C and D), ventromedial prefrontal cortex, posterior cingulate cortex (BA31) as well as fusiform and parahippocampal areas, bilaterally.

These data are consistent with recent single unit studies in monkeys reporting that abstract decision variables are represented in the dorsolateral prefrontal cortex and thus indicate that areas in human prefrontal cortex might indeed form a categorical decision by integrating evidence arriving from lower level areas (e.g. FFA, PPA) over time. To add evidence to these findings were are going to investigate this perceptual decision-making process with MEG and fMRI.

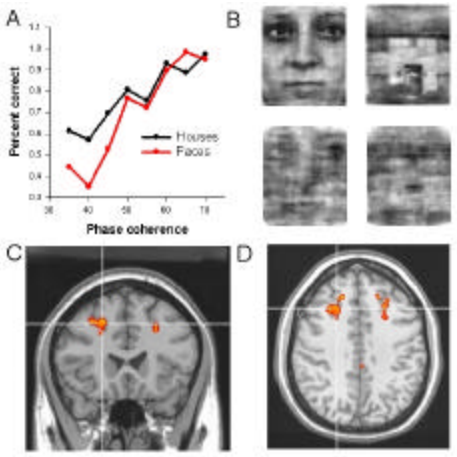

Fig 22: A. Behavioral pilot study showed that images of faces and houses with about 55% phase coherence were identified correctly with 82% probability. B. Scrambled images of faces and houses with same mean spatial frequency (upper row: high coherence, lower row: low coherence). C/D: Coronal (C) and axial view (D) showing prefrontal regions that covary significantly with the absolute signal difference between FFA and PPA. These data are consistent with recent single unit studies in monkeys reporting that abstract decision variables are represented in the dorsolateral prefrontal cortex and thus indicate that areas in human prefrontal cortex might indeed form a categorical decision by integrating evidence coming in from lower level areas (e.g. FFA, PPA) over time.

Acknowledgements

I would like to thank the past and present members of UFIM and FMRIF who have contributed their work and/or edits to this report. These include: James Patterson, Rasmus Birn, David Knight, Marta Maieron, Natalia Petridou, Hauke Heekeren, Sean Marrett, August Tuan, Jerzy Bodurka, Wen-Ming Luh, Frank Ye, Adam Thomas, Ziad Saad, Patrick Bellgowan, Karen Bove-Bettis, and Paula Rowser. I would also like to thank Kay Kuhns in assistance in preparation of summary materials– and practically every other administrative need in UFIM and FMRIF.

References

1. Rosen, B.R., et al., *Susceptibility contrast imaging of cerebral blood volume: human experience.* Magn. Reson. Med., 1991. **22**: p. 293-299.
2. Moonen, C.T.W., et al., *Functional Magnetic Resonance Imaging in Medicine and Physiology.* Science, 1990. **250**: p. 53-61.
3. Belliveau, J.W., et al., *Functional mapping of the human visual cortex by magnetic resonance imaging.* Science, 1991. **254**: p. 716-719.
4. Kwong, K.K., et al., *MR perfusion studies with T1-weighted echo planar imaging.* Magn. Reson. Med., 1995. **34**: p. 878-887.
5. Edelman, R., B. Siewert, and D. Darby, *Qualitative mapping of cerebral blood flow and functional localization with echo planar MR imaging ans signal targeting with alternating radiofrequency (EPISTAR).* Radiology, 1994. **192**: p. 1-8.
6. Kim, S.G. and N.V. Tsekos, *Perfusion imaging by a flow-sensitive alternating inversion recovery (FAIR) technique: application to functional brain imaging [published erratum appears in Magn Reson Med 1997 May;37(5):675].* Magnetic Resonance in Medicine, 1997. **37**(3): p. 425-35.
7. Wong, E.C., R.B. Buxton, and L.R. Frank, *Quantitative imaging of perfusion using a single subtraction (QUIPSS and QUIPSS II).* Magnetic Resonance in Medicine, 1998. **39**(5): p. 702-8.
8. Ogawa, S., et al., *Brain magnetic resonance imaging with contrast dependent on blood oxygenation.* Proc. Natl. Acad. Sci. USA, 1990. **87**: p. 9868-9872.
9. Turner, R., et al., *Echo-planar time course MRI of cat brain oxygenation changes.* Magn. Reson. Med., 1991. **22**: p. 159-166.

10. Kwong, K.K., et al., *Dynamic magnetic resonance imaging of human brain activity during primary sensory stimulation.* Proc. Natl. Acad. Sci. USA, 1992. **89**: p. 5675-5679.
11. Bandettini, P.A., et al., *Time course EPI of human brain function during task activation.* Magn. Reson. Med., 1992. **25**: p. 390-397.
12. Davis, T.L., et al., *Calibrated functional MRI: Mapping the dynamics of oxidative metabolism.* Proc. Natl. Acad. Sci. USA, 1998. **95**: p. 1834-1839.
13. Kim, S.-G. and K. Ugurbil, *Comparison of blood oxygenation and cerebral blood flow effects in fMRI: estimation of relative oxygen consumption change.* Magn. Reson. Med., 1997. **38**: p. 59-65.
14. Hoge, R.D., et al., *Linear coupling between cerebral blood flow and oxygen consumption in activated human cortex.* Proc Natl Acad Sci U S A, 1999. **96**(16): p. 9403-8.
15. Liu, T.T., et al. *A method for dynamic measurement of blood volume with compensation for T2 changes.* in *Proc., ISMRM 8th Annual Meeting*. 2000. Denver.
16. An, H., et al., *Quantitative measurements of cerebral metabolic rate of oxygen utilization using MRI: a volunteer study.* NMR Biomed, 2001. **14**: p. 441-447.
17. Das, A. and C. Gilbert, *Long-range horizontal connections and their role in cortical reorganization revealed by optical recording of cat primary visual cortex.* Nature, 1995. **375**(6534): p. 780-784.
18. Grinvald, A., et al., *Cortical point-spread function and long-range lateral interactions revealed by real-time optical imaging of macaque monkey primary visual cortex.* J. Neurosci, 1994. **14**((5 Pt 1)): p. 2545-2568.
19. Logothetis, N., et al., *Neurophysiological investigation of the basis of the fMRI signal.* Nature, 2001. **412**: p. 150-157.
20. Huettel, S.A. and G. McCarthy, *The effects of single-trial averaging upon the spatial extent of fMRI activation.* Neuroreport, 2001. **12**(11): p. 2411-6.
21. Saad, Z.S., Ropella, K. M., DeYoe, E. A., Bandettini, P. A., *The spatial extent of the BOLD response.* Neuroimage, in press.
22. Lee, A.T., G.H. Glover, and C.H. Meyer, *Discrimination of large venous vessels in time-course spiral blood-oxygen-level-dependent magntic-resonance functional neuroimaging.* Magn. Reson. Med., 1995. **33**: p. 745-754.
23. Rees, G., K. Friston, and C. Koch, *A direct quantitative relationship between the functional properties of human and macaque V5.* Nat Neurosci, 2000. **3**(7): p. 716-723.
24. Binder, J.R., et al. *Syllable rate determines functional MRI response magnitude during a speech discrimination task.* in *Proc., SMR, 2nd Annual Meeting*. 1994. San Francisco.
25. Rao, S.M., et al., *Relationship between finger movement rate and functional magnetic resonance signal change in human primary motor cortex.* J. Cereb. Blood Flow and Metab., 1996. **16**: p. 1250-1254.
26. Rees, G., et al., *Characterizing the relationship between BOLD contrast and regional cerebral blood flow measurements by varying the stimulus presentation rate.* Neuroimage, 1997. **6**(4): p. 270-8.
27. Boynton, G.M., et al., *Linear systems analysis of functional magnetic resonance imaging in human V1.* Journal of Neuroscience, 1996. **16**(13): p. 4207-21.
28. Friston, K.J., et al., *Nonlinear event-related responses in fMRI.* Magn. Reson. Med., 1998. **39**: p. 41-52.
29. Vazquez, A.L. and D.C. Noll, *Nonlinear aspects of the BOLD response in functional MRI.* Neuroimage, 1998. **7**(2): p. 108-18.
30. Albrecht, D.G., S.B. Farrar, and D.B. Hamilton, *Spatial contrast adaptation characteristics of neurones recorded in the cat's visual cortex.* Journal of Physiology, 1984. **347**: p. 713-739.
31. Bonds, A.B., *Temporal dynamics of contrast gain in single cells of the cat striate cortex.* Visual Neuroscience, 1991. **6**(3): p. 239-55.
32. Maddess, T., et al., *Factors governing the adaptation of cells in area-17 of the cat visual cortex.* Biological Cybernetics, 1988. **59**(4-5): p. 229-36.
33. Miller, K.L., et al., *Nonlinear temporal dynamics of the cerebral blood flow response.* Human Brain Mapping, 2001. **13**(1): p. 1-12.
34. Muller, J.R., et al., *Rapid adaptation in visual cortex to the structure of images.* Science, 1999. **285**: p. 1405-1407.
35. Mandeville, J.B., et al., *Dynamic functional imaging of relative cerebral blood volume during rat forepaw stimulation.* Magn. Reson. Med., 1998. **39**: p. 615-624.
36. Braddick, O.J., O'Brien, J.M., Wattam-Bell, J., Atkinson, J., Turner, R., *Form and motion coherence activate independent, but not dorsal/ventral segregated, networks in the human brain.* Curr Biol, 2000. **10**(12): p. 731-734.
37. McKeefry, D.J., et al., *The activity in human areas V1/V2, V3, and V5 during the perception of coherent and incoherent motion.* Neuroimage, 1997. **5**(1): p. 1-12.
38. Paradis, A.L., Cornilleau-Peres, V., Droulez, J., Van De Moortele, P. F., Lobel, E. , Berthoz, A. Le Bihan, D., Poline, J. B., *Visual perception of motion in 3-D structure from motion: an fMRI study.* Cereb Cortex, 2000. **10**(8): p. 772-783.
39. Rainer, G., et al., *Nonmonotonic noise tuning of BOLD fMRI signal to natural images in the visual cortex of the anesthetized monkey.* Curr Biol, 2001. **11**(11): p. 846-854.
40. Stroman, P.W., et al., *Extravascular proton-density changes as a non-BOLD component of contrast in fMRI of the human spinal cord.* Magn Reson Med, 2002. **48**(1): p. 122-7.
41. Bellgowan, P.S.F., Z.S. Saad, and P.A. Bandettini, *Understanding neural system dynamics through task modulation and measurement of fucntional MRI amplitude, latency, and width.* Proc Natl Acad Sci U S A, 2003. **100**: p. 1415-1419.
42. Friston, K.J., et al., *Stochastic designs in event-related fMRI.* Neuroimage, 1999. **10**(5): p. 607-19.
43. Dale, A.M., *Optimal experimental design for event-related fMRI.* Hum Brain Mapp, 1999. **8**(2-3): p. 109-14.
44. Liu, T.T., et al., *Detection Power, Estimation Efficiency, and Predictability in Event-Related fMRI.* NeuroImage, 2001. **13**(4): p. 759-773.
45. Birn, R.M., R.W. Cox, and P.A. Bandettini, *Detection versus estimation in event-related fMRI: choosing the optimal stimulus timing.* Neuroimage, 2002. **15**(1): p. 252-64.
46. Hu, X. and S.G. Kim, *Reduction of signal fluctuation in functional MRI using navigator echoes.* Magnetic Resonance in Medicine, 1994. **31**(5): p. 495-503.
47. Kruger, G. and G.H. Glover, *Physiological noise in oxygenation-sensitive magnetic resonance imaging.* Magn Reson Med, 2001. **46**(4): p. 631-7.
48. Bodurka, J. and P.A. Bandettini, *Toward direct mapping of neuronal activity: MRI detection of ultra weak transient magnetic field changes.* Magn Reson Med, 2002. **47**: p. 1052-1058.
49. Humphrey, D.E., *On the contribution of cell discharge and PSPs to the evoked potentials.* Clin Neurophysiol, 1968. **25**: p. 421-442.
50. Plenz, D. and S.T. Kital, *A basal ganglia pacemaker formed by the subthalamic nucleus and external globus pallidus.* Nature, 1999. **400**: p. 677-682.
51. Patterson, J.C., L.G. Ungerleider, and P.A. Bandettini, *Task-independent functional brain activity correlation with skin conductance changes: and fMRI study.* Neuroimage, 2002. **17**: p. 1787-1806.
52. Gold, J.I. and M.N. Shadlen, *Neural computations that underlie decision about sensory stimuli.* Trends Cogn Sci, 2001. **5**(1): p. 10-16.
53. Gold, J.I. and M.N. Shadlen, *Banburismus and the brain: decoding the relationship between sensory stimuli, decisions, and reward.* Neuron, 2002. **36**(2): p. 299-308.